Infrared Predissociation Spectroscopy of Large Water Clusters: A Unique Probe of Cluster Surfaces

C. Steinbach, P. Andersson,[†] J. K. Kazimirski, and U. Buck*

Max-Planck-Institut für Strömungsforschung, Bunsenstrasse 10, 37073 Göttingen, Germany

V. Buch

The Fritz Haber Institute for Molecular Dynamics, The Hebrew University, Jerusalem 91904, Israel

T. A. Beu

University "Babeş-Bolyai", Faculty of Physics, RO-3400 Cluj-Napoca, Romania

Received: February 17, 2004; In Final Form: May 13, 2004

The vibrational OH-stretch spectra of large water clusters were measured by photofragment spectroscopy after the absorption of pulsed tunable infrared radiation in the frequency range from 3000 to 3800 cm^{-1}. The mean size of the clusters from $\langle n \rangle = 20$ to 1960 was measured by threshold photoionization of the water clusters doped with sodium atoms. The largest abundance of the fragments was that of water hexamers. The fragment intensities are measured for different excitation energies and different cluster temperatures as function of the cluster size. For the selected sizes $\langle n \rangle = 48$, 111, 631, and 1960 complete OH-stretch spectra have been measured. The comparison with calculations revealed that the method is mainly sensitive to the outer cluster surface which has for all sizes an amorphous structure dominated by 3-coordinated and to a lesser extent also by 4-coordinated molecules. The intensity of the hexamer fragments goes through a maximum at $n = 70$ and drops to $n = 300$ where it levels off with a different slope. This behavior is attributed to the number of available connected 3-coordinated water molecules and the influence of the emerging 4-coordinated molecules in these clusters.

I. Introduction

The condensed phase of water is still, after so many years of intensive research, the objective of many investigations and attracts the interest of numerous scientists. The reasons are obvious. On one hand, water plays a key role as ubiquitous solvent and as promotor of many reactions in atmospheric and space chemistry. On the other hand, the many anomalous properties of the liquid and the solid water in its different crystalline ice configurations and in the phase of amorphous solid water (ASW) make this hydrogen bonded network so interesting. For several years, water clusters in the gas phase have had an increasing influence on the elucidation of these intrinsic properties. First, some of the experimental results are well defined, easy to obtain, and are not hampered by complicated averaging processes. Second, the variation of the cluster size allows us to investigate experimentally the development of properties of the condensed phase in a step-by-step manner. Third, the finite number of molecules in a well-defined environment makes a theoretical treatment easier than that of the bulk liquid or solid.

In this respect, the spectroscopy and here, in particular, the vibrational spectroscopy of the OH stretch mode is quite a sensitive method to determine directly the strength and the coordination of the hydrogen bonded network. This mode is shifted up to 800 cm^{-1} to the red from the positions of the symmetric and asymmetric stretch vibrations of the free water molecule at 3655 and 3756 cm^{-1}, respectively, depending on the direct and also the more distant neighbor molecules. Typical results are the IR spectrum of liquid water exhibiting a broad, unstructured distribution with a maximum at 3400 cm^{-1} (refs 1, 2), whereas the spectrum of amorphous solid water, ASW, shows a similar distribution peaked at 3270 cm^{-1} (ref 3). Here, the additional red shift is an indication of the stronger hydrogen bonds in the solid, while the width of the distributions can be traced back to the disorder of the O atoms.[4] Finally, hexagonal ice displays a somewhat smaller distribution, peaked at 3220 cm^{-1} with shoulders at 3100 and 3380 cm^{-1}.[3] The remaining broadening is attributed to the inter- and intramolecular coupling between OH bonds in the proton-disordered crystal.[5]

In contrast, the spectra of small water clusters in the size range from $n = 2$ to $n = 10$ consist of well separated lines which can all be ascribed, with the help of calculations of the cluster structures and their IR spectra, to their specific environments.[6−13] It includes the free OH stretch mode at 3695 to 3720 cm^{-1}, depending on the adjacent molecules, and the 2-coordinated hydrogen bonded DA modes (one donor and one acceptor) which occur in cyclic structures at 3533, 3416, and 3360 cm^{-1} for the trimer, tetramer, and pentamer, respectively. In the size range from $n = 7$ to 10 with three-dimensional structures that are derived from the octamer cube by subtracting and adding molecules,[10,14] 3-coordinated single donors (DAA) at 2950 to 3100 cm^{-1} and double donors (DDA) around 3550 cm^{-1} are observed. The hexamer is the first three-dimensional structure with a large variety of nearly isoenergetic isomers[15−18]

* Corresponding author. E-mail: ubuck@gwdg.de
† Present address: Department of Chemistry, Physical Chemistry, Göteborg University, SE-412 96 Göteborg, Sweden.

which range from the cage[19] over the ring[20] to the book.[21] Thus we get from the OH stretch modes of these clusters a one-to-one correspondence between wavenumbers and coordination, which can serve as fingerprints for further identification in larger systems. In addition, the high resolution rotational−vibrational tunneling spectra from the dimer to the hexamer provide similar conclusions about the structures.[22−25] The results of the dimer have been used to derive very accurate two-body interaction potentials for water.[26] Similar results have been obtained by adding an aromatic chromophore to the water clusters. Results are available for benzene−water,[27−30] phenol−water,[31−33] and other substituted benzene−water[34] systems.

In the size range for $n = 11-30$, a series of calculations is available that can be viewed as multiple fused cage structures.[35−42] In this size range and the one that follows, up to several hundred molecules, only a few measurements are available for which, in addition, the sizes are not known. In these papers, aside from the isolated peak of the free OH stretch around 3720 cm^{-1}, mainly broad distributions were measured.[43−48] For still larger clusters, the range of ice nanoparticles, considerable experimental and computational information is available. The electron diffraction studies revealed the crystalline diffraction pattern of cubic ice.[49−51] For smaller clusters the presence of an amorphous component was observed.[49] For particles in the size range from 3 to 60 nm the Fourier transform infrared (FTIR) absorption spectroscopy in cold condensation cells, in conjunction with computations, revealed an interesting behavior.[52−57] The particles in this size range for cluster sizes $n \geq 400$ consist of a crystalline core and an amorphous surface that is traced back to the nearly spherical shape of these objects. In clusters including several hundred molecules, the crystal core is strained by the interaction with the disordered surface.[57]

In the present contribution we address cluster sizes in the broad range between the lower tens to several thousands using two novel techniques that allow us (i) to work with known average sizes and (ii) to apply a kind of IR spectroscopy, which proved to be mainly sensitive to the surface of these clusters. The sizes are determined by doping the clusters with single Na atoms, which are detected nearly fragmentation-free by photoionization close to the threshold.[58] For the IR spectroscopy of the OH stretch mode we have chosen the fragment spectroscopy,[43,59] since the well established depletion technique that was successfully used in the spectroscopy of completely size selected small water clusters[6,10,60] is not adequate for large clusters. We detected mainly larger fragments up to $(H_2O)_4H^+$ that proved to be sensitive to the cluster surface. Results will be presented for the average cluster sizes $\langle n \rangle = 48, 110, 631$, and 1960. They will be compared with calculated spectra that have been obtained from low energy structures for $n = 48$, $n = 123$, and $n = 931$.[56,61] For $n = 600$ new calculations were carried out in this paper. A preliminary account of the experimental results has been published in conference proceedings.[62,63]

In section II we will give a brief description of the experimental setup. In section III we will discuss the experimental methods, which include the angular and size dependence of the different fragments and their sensitivity to the location and the structure of the clusters. Then we present the theoretical methods with the calculation of the IR spectra included in section IV. The results with the comparison of measured and calculated spectra and the relation to the cluster structure are discussed in section V. The summary and concluding remarks are presented in section VI.

TABLE 1: Beam Data

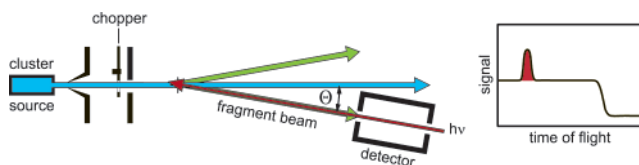| property	exp 1	exp 2	exp 3	exp 4
diameter of conical nozzle d (μm)	90	60	50	50
angle 2β (degree)	30	20.4	41	41
length (mm)	2	6	2	2
nozzle temperature (K)	355	495	495	495
pressure (bar)	2.3^a	3.0	11.0	21.0
average size $\langle n \rangle$	40	111	631	1960

^{a} 16.7% mixture in helium.

Figure 1. Schematic view of the experimental setup for measuring photo fragment spectra.

II. Experimental Section

The experiments have been carried out in a molecular beam machine that has been described in detail previously.[64,65] The large water clusters are produced in a supersonic expansion of mixed and pure water vapor at 2 to 22 bar through nozzles of conical shape with diameters between 50 and 90 μm, opening angles between 20° and 41°, and 2 to 6 mm length. The actual parameters are listed in Table 1. The average size of the resulting cluster distribution is determined by applying the recently developed method of doping the cluster by the pick-up of Na atoms.[58] In this way the cluster can be ionized free of fragmentation by single photons close to the threshold, since the ionization potential is significantly reduced to 3.2 eV and can thus be easily reached by a dye laser. The vibrational spectra of the pure large water clusters $(H_2O)_n$ are measured in the schematic experimental arrangement depicted in Figure 1. The pulsed infrared optical parametric oscillator (OPO) output crosses the cluster beam in a quasi-collinear configuration under a small angle and is tuned in a frequency range of 3000−3800 cm^{-1} with a bandwidth of 0.2 cm^{-1}. The laser fluence varied from 100 to 500 mJ/cm^2 in a single pulse. If a vibrational mode of the clusters is excited, the energy is redistributed and leads to the decay of the cluster. For small water clusters this decay is usually detected by the depletion of the signal.[6,14] This method is not very suitable for large clusters, since the change in the signal is quite small. Here the detection of the fragment is much more appropriate. Therefore the detector, a rotatable quadrupole mass filter with a continuous electron bombardment ion source, is positioned at an angle Θ of about 2.0−4.5° with respect to the water cluster beam. A chopper allows digital lock-in (DLI) measurements, to discriminate the signal of the continuous water cluster beam from background. Neutral fragments are leaving the clusters and thereby diverging from the direction of the water cluster beam. Therefore, they are detected as enhancement of the signal following the laser pulse in the time-resolved ion signal of the tuned masses.

III. Experimental Results

A. Cluster Sizes. The average size of the cluster distribution is determined by applying the recently developed method of doping the cluster by the pick-up of Na atoms.[58] In this way the cluster can be ionized free of fragmentation by single photons close to the threshold, since the ionization potential is significantly reduced to 3.2 eV. In the present experiment the photoionization takes place by a dye laser operated at the wavelength of 360 nm (3.46 eV). A typical result is shown in
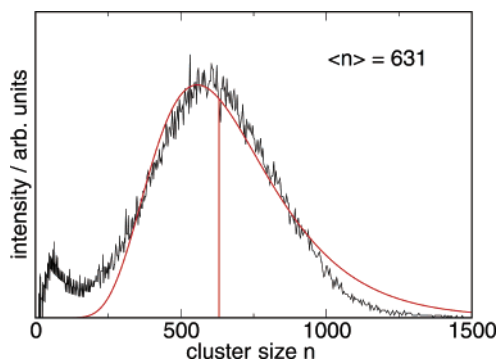
Infrared Predissociation Spectroscopy

J. Phys. Chem. A, Vol. 108, No. 29, 2004 **6167**

Figure 2. Measured mass distribution of water clusters with the mean size $\langle n \rangle = 631$ indicated by the vertical line. The solid line is a log-normal distribution fitted to the measurement.

Figure 2 for the experimental conditions of the experiment (3) in Table 1. The solid line is a fit to the experimental data using the log-normal distribution

$$f(n) = \frac{1}{\sqrt{2\pi}\sigma n} \exp\left[-\frac{(\ln n - \mu)^2}{2\sigma^2}\right] \qquad (1)$$

with the two parameters μ, the logarithm of the geometric mean, and σ, the logarithm of the geometric standard deviation. The mean cluster size of $\langle n \rangle = 631$, which is also marked in the figure, is directly determined from the fit.

Based on a series of such results we have derived a scaling law[58] that relates the mean cluster size $\langle n \rangle$ to the source conditions of the expansion in the spirit of the well-known scaling laws derived by Hagena for rare gases and metals.[66,67] The key parameter that correlates the flow that produces the same cluster size is given by

$$\Gamma = n_0 d^q T_0^\alpha \quad (0 < q \leq 1) \qquad (2)$$

Here n_0, T_0, and d are the source density, nozzle temperature, and nozzle diameter. For water clusters we get $q = 0.643$ and $\alpha = -2.655$. For nozzles with conical shape and an opening angle of 2β, the nozzle diameter d has to be replaced by $d_{eff} = 0.933/\tan\beta$. It is convenient to reduce the length and energy scale by introducing the reduced parameter $\Gamma^* = \Gamma/(r_{ch}^{q-3} T_{ch}^\alpha)$ with $r_{ch} = 3.19$ Å and $T_{ch} = 5684$ K. Then we are able to present the relation of the average cluster size $\langle n \rangle$ with the reduced source parameter Γ^* by a simple power law:

$$\langle n \rangle = D\left(\frac{\Gamma^*}{1000}\right)^a \qquad (3)$$

with $D = 2.63$ and $a = 1.872$. In this way the sizes of water clusters generated in adiabatic nozzle expansions can be calculated from the source parameters.

B. Dissociation. The pulsed infrared radiation excites the OH stretch vibrational modes of the water clusters and the resulting predissociation is detected by the outgoing fragments. A typical angular distribution of the fragments is shown in the upper part of Figure 3. The mean cluster size of the water cluster beam was $\langle n \rangle = 300$, and the excitation occurred at 3718 cm^{-1}, the position of the free OH stretch motion of the water clusters. The rapid fall off and the peaking at 0° is an indication of very small translational energy and large internal excitation. As expected from the kinematics of the reaction, the smaller fragments are scattered into larger angles as is manifested by the flatter slope. The most remarkable result, however, is the high intensity of the heavier fragments $(H_2O)_kH^+$ with $k = 2$ to
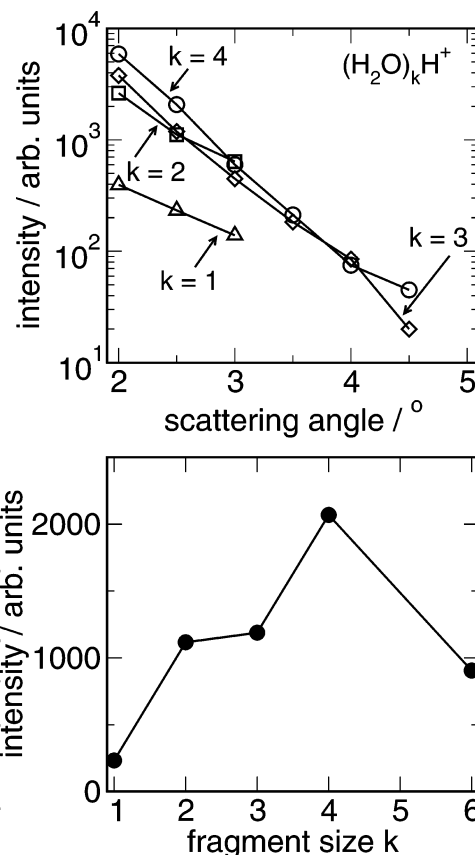

Figure 3. (upper panel) Measured angular dependence of the indicated ion signals $(H_2O)_kH^+$ at the mean cluster size of $\langle n \rangle = 300$ and a wavelength of 3718 cm^{-1} (free OH). (lower panel) measured dependence of the fragment size k taken at the deflection angle of 2.5°. We note that the corresponding parent clusters have usually larger masses because of fragmentation in the ion source.

4 with respect to H_3O^+. This is displayed in the lower panel of Figure 3 for a fixed angle. The species with the largest intensity is that with $k = 4$. At both ends of the investigated fragment masses the intensity is smaller. If we take into account the well-known fragmentation[68] of the water clusters by electron impact ionization, where in addition to the protonation at least one monomer is lost for systems larger than the dimer, we have the surprising result that fragments of the neutral precursor hexamer, and to a lesser extent also those of the pentamer and tetramer, are much more frequent than those of the dimer. This result is not what one would expect when energy is statistically distributed in a cluster. In such a case, the smallest fragments should be ejected with the largest probability. Such a result has been measured in the IR spectroscopy of pure[43] and methanol-doped[59] water clusters. According to our relations of source conditions and cluster sizes,[58] presented in the last section, the water cluster sizes in these experiments did not exceed the average size of $\langle n \rangle = 20$. Therefore, the results of the present measurements might be traced back to the larger cluster sizes.

For these reasons, we calculated the fragmentation of large water clusters, $n = 100$ and $n = 1000$, by molecular dynamics (MD) simulations. The details of the calculations and the results are described in the appendix. For the excitation mechanism we used the simplest model available, the local heating of the cluster by increasing its temperature. Whatever was varied — surface or inner position of the excitation, different temperatures, and different clusters sizes — the results exhibited always a similar general feature. Although fragments up to the size of $s = 10$ were observed, the fragment distributions were dominated
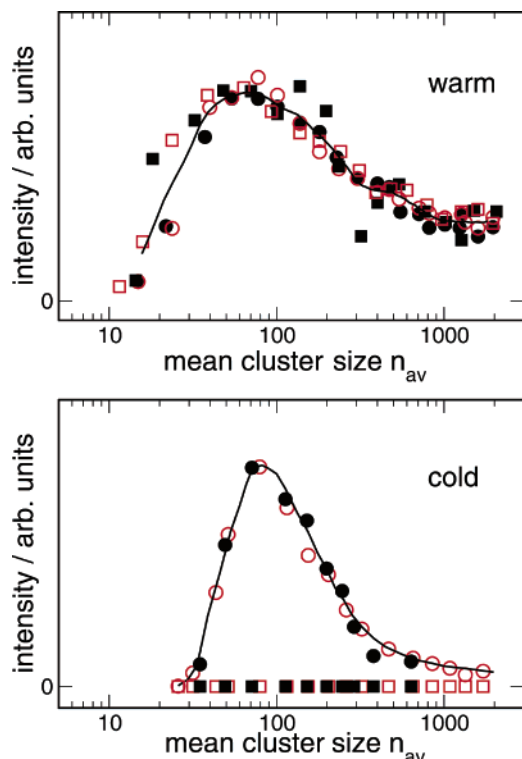
Figure 4. Cluster size dependence of the OH stretch intensity taken at 3718 cm^{-1} (full characters) and 3200 cm^{-1} (open characters) at the mass $(H_2O)_4H^+$ (circles) and $(H_2O)H^+$ (squares) for different temperatures.

by small fragments with an exponential fall off toward larger fragments. In contrast to the fragmentation caused by collisions of high energy electrons with water and other clusters, which could be correctly predicted by MD simulations,[69] the measured interaction of IR photons within this hydrogen bonded network as was measured in the present contribution is not reproduced by such a simplified scheme.

What is primarily not explained by the simulation is the reversed intensity distribution of the fragments observed in the experiment and shown in Figure 3. Apparently, a mechanism other than the heating of all degrees of freedom is operating here. In the vibrational predissociation of binary complexes, the coupling of the vibrational motion with the free translational motion in the dissociation continuum leads to the momentum gap law which states that the translational motion of the product is minimized at the expense of the excitation of the next lying internal state.[70−72] In a system with many more internal degrees of freedom, such as in large water clusters, the lifetime of the system is composed of two contributions.[43] (i) The first is the energy transfer from the initially excited *intra*molecular modes into the *inter*molecular cluster modes. Here the coupling between these two groups of states plays a crucial role. (ii) The next step is the decay of the excited cluster along the intermolecular coordinates and the subsequent evaporation of products after the energy is distributed throughout the cluster.

To get more experimental information on this problem we have measured the dependence of two characteristic fragment signals, $(H_2O)_4H^+$ and H_3O^+, on the cluster size. The experiments are carried out for two different wavelengths, 3718 and 3200 cm^{-1}, which correspond to the free and hydrogen bonded OH stretch modes. The results are presented in Figure 4. In addition to the variables already discussed, the measurements were conducted for two different cluster temperatures. This was

achieved by using two different lengths of the conical shaped nozzle under otherwise similar conditions. The longer conical nozzle leads to a substantially longer interaction time before the zone free of interaction is reached. The cooling by collisions with the remaining monomers is more effective and we estimate a colder cluster temperature in this case. Therefore, the results obtained with the different nozzles are marked with "warm" in the upper panel and "cold" in the lower panel.

Let us summarize the results presented in Figure 4 as follows. (1) There is, in general, no difference in the results for the two laser excitation energies. (2) We observe a pronounced size dependence of the $(H_2O)_4H^+$ signal and cold clusters. The distribution rises from $\langle n \rangle = 30$ to a peak at about $\langle n \rangle = 70$, and falls off to about $\langle n \rangle = 300$ where a change in the slope is observed. (3) In the case of the warm clusters, the distribution is broader, the maximum is the same, and the tail with the different slope exhibits higher intensities. (4) The H_3O^+ signal is zero for the cold cluster temperature and follows, for the warm cluster, with some deviations the general trend of the heavier fragment.

The step from the cold to the warm cluster is easy to understand. The higher internal energy leads to an easier dissociation and thus the intensity at small and large sizes increases and the general curve is broadened. What is more difficult to recognize is the effect which we already observed in the measurement of the angular dependence in Figure 3, the distinct preference of the larger fragments compared to the dimer for cold clusters.

The other remarkable feature is the pronounced size dependence of the intensity. If we consider the energetic conditions for the production of larger fragments, say hexamers, we find that for 4-coordinated molecules 12 bonds have to be broken, while this number is 6 for 3-coordinated molecules. Here we anticipate that 2-coordinated hexamers are formed. Thus 3-coordinated molecules should be energetically favored. Let us consider the number of 3-coordinated molecules. It increases with increasing cluster size in this regime of amorphous cluster structures. Based on the results of ref 56, we estimate ≈21 3-coordinated molecules for $n = 48$ and ≈42 for $n = 123$. This trend, however, continues, although somewhat weakened, for $n = 293$ where ≈66 3-coordinated molecules are counted. According to this behavior we would expect a continuous increase of the intensity. Apparently, the intensity decreases after $n = 70$. Aside from the 3-coordinated molecules we find also 4-coordinated molecules at the surface. In the investigated size range from $n = 22$ (ref 56), $n = 48$ (ref 56), and $n = 90$ (ref 73) the ratio $R(3/4)$ of 3- to 4-coordinated molecules varies between 1.2 and 0.97. For larger values it drops to $R(3/4) = 0.78$ for $n = 123$, and finally to $R(3/4) = 0.48$ for $n = 293$ (ref 56). A related observation pertains to connected groups of low-coordinated molecules on the surface. The percentage of 3-coordinated molecules participating in groups of 4 to 7 members is 35~40% for $n = 48$ and $n = 123$, dropping to ≤10% in clusters with several hundred molecules. Thus, it becomes more and more difficult for the 3-coordinated molecules to form the larger complexes. At about $n = 300$ the curves in Figure 4 level off and change the slope. This size range is known from previous analysis to be the onset of the crystalline core.[54,56,57] We will discuss the influence of the different parts later after we have established by comparison with calculations the part of the cluster to which the measurements are precisely sensitive.

Infrared Predissociation Spectroscopy

J. Phys. Chem. A, Vol. 108, No. 29, 2004 **6169**

IV. Theoretical Methods and Results

The methodology for locating low energy cluster structures and for calculating spectra, as well as computational results for the range of tens to hundreds of water molecules, will be described in detail in a separate publication.[61] A brief summary pertinent to the present experimental results is given below.

For $n = 48$ and 123 we employ low energy structures located in a recent optimization study.[56] The optimization procedure combined temperature dependent classical trajectories, hydrogen network improvement, and optimization by diffusion Monte Carlo. This scheme was shown to lower effectively the energy of the particles. However, in the pertinent size range, finding the ultimate lowest energy cluster structure is very difficult, because of a multitude of minima separated by relatively high barriers; thus our more modest and general goal has been the location of "typical" low energy structures, as function of size. For $(H_2O)_n$, $n = 48$ and $n = 123$, the optimized lowest energy structures were compact, 3-dimensional, and *amorphous*. Structures with these final characteristics were obtained for $n = 48$ starting from a number of initial conditions which include tubes of four- and six-membered rings, sandwich structures, a spheroid shape cut from a crystal, and frozen amorphous droplet. The last two yielded compact amorphous structures of very similar energies and similar qualitative structural characteristics. The tubes and the sandwich yielded a significantly higher energy. These results suggest amorphous compact cluster structures. For $n = 123$ the procedure and the results were similar, except that we did not try any tubes or sandwiches; the preference for compact three-dimensional structures is expected to increase with size.

In contrast, at $n = 293$, optimized structures obtained starting from a cut out spherical cubic ice crystal[49−51] were significantly lower in energy than those obtained starting from amorphous initial conditions ("frozen droplet"). Numerical experiments to construct shapes enclosed by crystal surfaces but then deviating from spherical shape gave an increased energy. Quasi-spherical shapes give minimal surface area, and the dangling O- and H-atoms recombine quite effectively. The final optimized structure included a largely crystal core and a disordered surface; however, the core was strained significantly by the interaction with the surface. The ice crystal structure is favorable for the interior rather than for the surface, and therefore a minimum cluster size is required for crystallinity. The present results indicate that the crystallization threshold is above the size $n \sim$ 100. The surface adopts a non-crystalline disordered structure with enhanced population of five- and four-membered water rings, which allow for reduction in the population of undercoordinated surface molecules. Additional calculations were carried out recently for $n = 600$ and $n = 931$. Due to the size of the problem, only the first step of the optimization procedure (temperature-dependent trajectories) was applied. The pattern of dangling-O and dangling-H atoms on the surface may not be optimal, as a result.[56] But again, the general optimized structures, which included a crystal core and a disordered surface as shown in Figure 5 for $n = 600$, should be reliable. These larger sizes are associated with the appearance of *unstrained* crystal ice in the interior.[54,55,57] The above structural evolution is in accord with past analysis based on FTIR investigations for $n = 400$ to $\sim$1,000,000, and computational modeling of $(H_2O)_{979}$.[54,55,57]

For the above optimized structures, the spectra were calculated quantum mechanically using a model devised in the past.[11,14,52,54] OH bonds are treated as local Morse oscillators. The ground state is approximated as a product of ground Morse
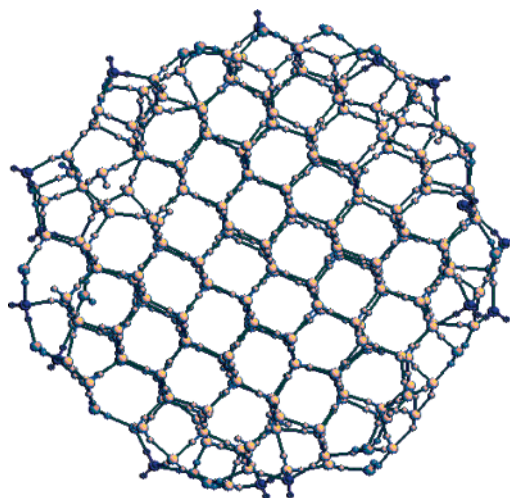

Figure 5. Center slice through the calculated structure of $(H_2O)_{600}$.

states for all the OH bonds. An excited state is expanded in the exciton basis $\sum c_i |1_i\rangle$, where $|1_i\rangle$ is a product basis state with one quantum in bond i and zero quanta in the remaining bonds. The intermolecular OH···OH coupling is modeled as oscillating dipole−oscillating dipole interaction. The intramolecular coupling is a sum of momentum coupling between two OH bonds sharing an O-atom, and a potential coupling bilinear in bond stretch coordinates. The bond frequency ω is assumed to be determined by the electric field component $E_{\parallel}$ at the H-atom along the OH bond, as suggested by ab initio studies of ref 74. The field is calculated at a cluster minimum, using the permanent charges and the induced dipoles of the polarizable potential EMP.[75] The function $\omega(E_{\parallel})$ was constructed by fitting experimental IR spectra at two size limits ($n = 8$ and $n = 931$).[14,54] Because of the relatively large size of clusters considered in this study, the simplest version of the algorithm was employed, which did not include the effects of coupling between inter- and intramolecular vibrations on the spectra. The model yielded semiquantitative agreement with FTIR spectra of ice and of ice nanoparticles.[5,54,55]

The calculated spectra for two selected cluster sizes $n = 48$ and $n = 931$ are depicted in Figure 6. The spectra of the complete cluster, the black lines in Figure 6a and c, show a characteristic shift in the maximum intensity from about 3300 cm^{-1} to below 3200 cm^{-1}. The analysis of the corresponding coordinations, shown in Figure 6b and d, exhibits that mainly 4-coordinated molecules are the origin of these peaks. To get information on 3-coordinated molecules one has to look for surface spectra of the larger clusters $n = 931$ or at the extreme ends of the spectrum of the smaller cluster $n = 48$, as is demonstrated by the colored lines in Figure 6a and c.

V. Comparison of Measured and Calculated Spectra

Now we measured the vibrational predissociation spectra in the full wavenumber range of 3000 to 3800 cm^{-1}, which covers the complete OH stretch excitation. The average cluster sizes, which are determined by the doping method with sodium atoms[58] as was described in section III A, include $\langle n \rangle = 40$, 111, 631, and 1960. The data were, in general, taken at the mass of the fragment ions $(H_2O)_4H^+$, which we attribute to the neutral water hexamers $(H_2O)_6$. In the case of the largest cluster $\langle n \rangle = 1960$, we also detected the $(H_3O)^+$ fragment which is attributed to the dimer. The spectra of the two smaller sizes are taken in the configurations exp 1 and 2 of Table 1, which produce cold clusters, while those of the larger sizes are
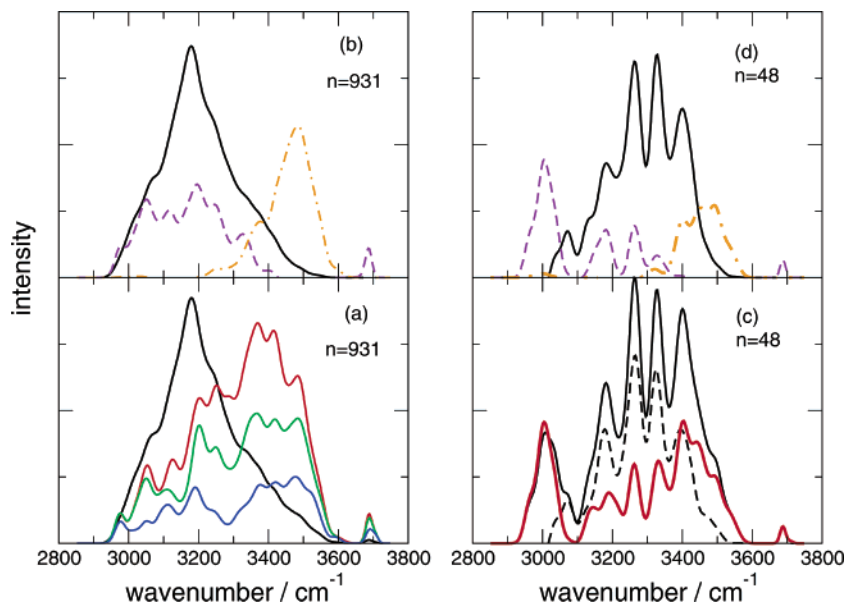
Figure 6. Calculated spectra, for lowest energy configurations found for $n = 931$ (quasi-spherical structure, crystal core, disordered surface), and $n = 48$ (compact, amorphous three-dimensional structure). (a) $n = 931$; black: total calculated spectrum; blue, green, and red: surface spectra, including contributions of molecules in the surface layer at a distance $r > r_c$ from the cluster center of mass, with $r_c = 18.5, 18, 17.5$Å, respectively. The total spectrum was reduced by a factor 0.12 to enable comparison to surface spectra. (b) $n = 931$, contributions of different coordinations: violet, dashed − DAA molecules; orange, dot−dashed − DDA molecules; black − DDAA 4-coordinated molecules (spectrum reduced by a factor 0.12). (c) $n = 48$, black, solid: total spectrum; red: external layer $r > 5$Å, black, dashed: interior contribution. (d) $n = 48$, contributions of different coordinations, notation as in (b).

generated by warm clusters. The experimental results of these OH-stretch spectra are depicted in Figure 7. The gap around 3500 cm^{-1} of the measured points is an artifact of the experimental arrangement. The crystal used in the OPO has a water impurity in this frequency range and does not amplify IR radiation. The spectra are dominated by peaks at 3720 and 3550 cm^{-1} for all sizes and a variable peak moving from 3420 to 3350 cm^{-1} for the smaller clusters, which is marked by a solid line. Peaks in this range continue to be present also for the larger clusters. The larger clusters exhibit, in addition, a peak with increasing intensity near 3220 cm^{-1} that is not present for the smaller clusters. Those exhibit, in contrast, peaks below 3200 cm^{-1}.

We note that the amplitudes in these measurements do not necessarily reflect the IR absorption cross sections, but are the product of these with the coupling of the respective intramolecular motions to intermolecular excitation along the H bonds leading to the dissociation of the clusters.[76] In fact, there is qualitative disagreement between the experimental spectra in Figure 7 and the calculated spectra for the entire cluster, in Figure 6 (a and c, black solid curves). The computed spectra reflect infrared absorption intensity, and weighting by dissociation probability is not included. The discrepancy is especially striking for the larger cluster size, for which the calculated bonded-OH band peaks at 3200 cm^{-1}, while the experimental one extends, with relatively modest variation of intensity, from ~3100 to 3600 cm^{-1}. One may note that the computed whole-cluster spectra are in qualitative agreement with the experimental FTIR spectra obtained in a cold condensation cell.[55,57,61]

On the other hand, much better agreement is obtained while comparing the predissociation spectra with the computed *surface* spectra of Figure 6; the latter were obtained by including only contributions from surface molecules, whose distance from the cluster center of mass exceeds some cutoff radius r_c. The computed distribution of molecules of different coordinations as a function of distance from the cluster center-of-mass is shown in Figure 8 for two selected sizes; not unexpectedly, low
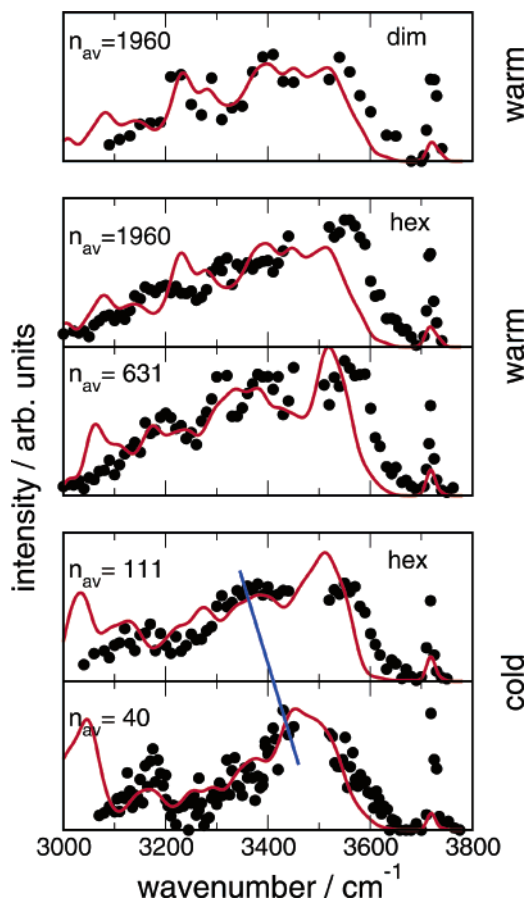

Figure 7. Measured OH stretch fragment spectra (full points) detected at $(H_2O)_4H^+$ (hex) and $(H_2O)H^+$ (dim) for the average cluster sizes indicated. The spectra were taken at different temperatures marked on the right-hand side. Trends are indicated by a straight line. The continuous lines are calculated surface spectra for $n = 48, 123, 600,$ and 931.
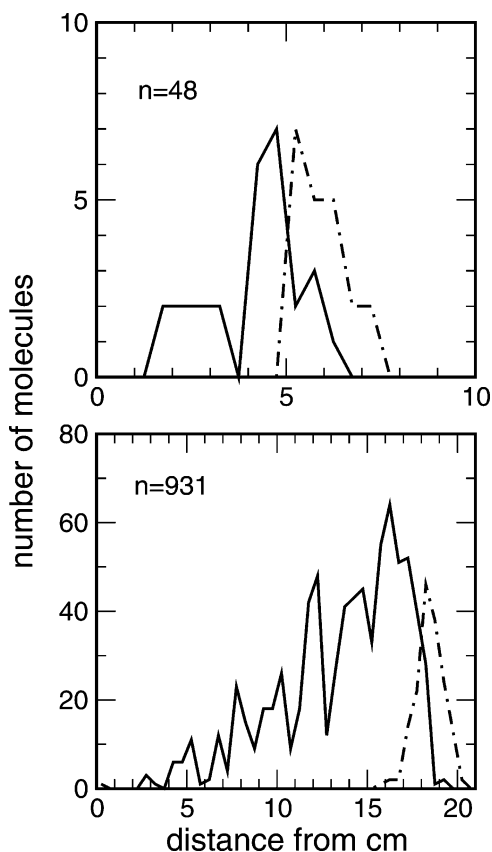
Infrared Predissociation Spectroscopy

J. Phys. Chem. A, Vol. 108, No. 29, 2004 **6171**

Figure 8. Distribution of distances from cluster center of mass, for lowest energy structures found for $n = 931$ and $n = 48$. Solid: coordination ≥ 4 (mostly 4-coordinated); dot—dashed: coordination ≤ 3 (mostly 3-coordinated).

Figure 9. Comparison of calculated surface spectra of $n = 931$ from Figure 6 for different cutoffs $r_c = 18.5$ Å for the dimer signal and $r_c = 17.5$ Å for the hexamer signal with the top two spectra of Figure 7. For details of the experiment see caption of Figure 7.

coordinated molecules are concentrated in the outer surface. The values of r_c which result in qualitative agreement with the predissociation experiment are near a distance at which 3-coordinated molecules start dominating the distribution (i.e., at a point at which the dot—dashed curve crosses the solid curve, 5 Å for $n = 48$, and 18 Å for $n = 931$).

The direct comparison of the measurements with the surface spectrum calculated in this way is also shown in Figure 7 by the solid lines. We note that for $n = 48$ and 123 the spectra are averaged over a couple of close lying low energy isomers so that some of the structure displayed in Figure 6c is washed out. For $n = 48$ and $n = 123$ the spectra were averaged over 10 lowest lying configurations, which were found using the TIP4P potential.[77] The minima are different but qualitatively similar (amorphous compact). For $n = 600$ and $n = 931$, the lowest energy structure found was used. While measured and calculated (in parentheses) sizes agree very well for $\langle n \rangle = 40$ ($n = 48$), $\langle n \rangle = 111$ ($n = 123$), and $\langle n \rangle = 631$ ($n = 600$), the data for $\langle n \rangle = 1960$ had to be compared with the calculations for $n = 931$. This difference is, however, not so important since in this size range the cluster structure is very similar. The only adjustment that has been made in this comparison is to shift the complete spectrum by 32 cm^{-1} so that the position of the free OH stretch mode is matched. The overall agreement between experiment and calculations is remarkable. Deviations occur for the free OH in the intensity of the peaks. There are also small shifts in the positions around 3550 cm^{-1} and more pronounced peaks in the calculation in the range around 3100 cm^{-1}.

To improve the agreement with the two top experimental spectra in Figure 7, we have compared the results with computed spectra corresponding to different cutoff distances as are
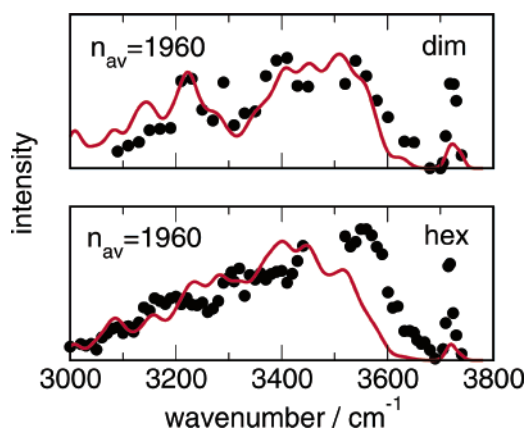
obtained in Figure 6a. The direct comparison is presented in Figure 9. The dimer spectrum matches better the calculation for $r_c = 18.5$ Å, while the hexamer spectrum agrees better with $r_c = 17.5$ Å. This suggests that dimers emerge from the very top of the surface layer, while the excitation depth for producing hexamers is somewhat larger.

We are now able to assign the peaks in the experimental spectra based on the calculation in Figure 6 (b,d). In accord with past studies,[14,52] the free OH of DAA molecules gives rise to the narrow highest frequency band, while the bonded OH of the DAA molecules dominates the low-frequency end of the spectrum. At $n \sim 40$, DAA molecules give rise to a prominent, separate band at the low frequency end of the spectrum both in experiment and in calculation, although the computed frequency is lower (the discrepancy is most likely due to approximations of the computational model). At larger sizes, the bonded DAA spectrum peaks at a higher frequency, ~ 3220 cm^{-1}; the corresponding peak is visible in the dimer spectrum (see Figures 6, (b,d), and 9). DDA molecules dominate the high-frequency end of the bonded OH band.

We conclude that the experimental method is essentially sensitive to the outer surface of the cluster. We do not know the exact molecular level details of the process that removes clusters from the $(H_2O)_n$ surface via photoexcitation. However, it stands to reason that the process is dominated by excitation of the most weakly bonded low-coordinated molecules, which constitute the interface with the vacuum. This is also in agreement with the considerations in section III B which pose that mainly the energetically favored 3-coordinated molecules are responsible for the measured size dependence of the intensity of the photoproducts in Figure 4. This region is amorphous over the whole size range investigated. Thus, the fragment spectroscopy of the hexamer occurs only in an amorphous environment.

As was mentioned earlier, the coupling of originally excited intramolecular vibrational modes to the number of intermolecular states is crucial for the step (i) in the dissociation mechanism. This number is usually higher for amorphous solid water than for crystalline hexagonal ice because of the broader distribution of the density of states in the whole range of intermolecular motions down to the low energy range of the translation and librational modes.[78] A similar behavior has been observed in the vibrational relaxation of the OH-stretch mode in liquid water where the dominant accepting channel was the hydrogen bonds.[79] This behavior explains the preference of the amorphous structure.

Finally, we have to explain the shape of the curve for the size dependence in Figure 4 with the maximum at $n = 70$ and the leveling off at about $n = 300$, which coincides with the onset of the appearance of a crystalline part in the cluster.[54,56,57] The photoproducts consist mainly of 3-coordinated molecules out of the outer surface layer. The density of these molecules turned out to change only weakly with size. What really counts are connected groups of under-coordinated molecules. As was already mentioned, the percentage of 3-coordinated molecules in such connected groups with four to seven members is 43% for $n = 48$, 33% for $n = 123$, 9% for $n = 293$, and 10% for $n = 600$. Although the data are scarce and we do not have models close to the maximum at $n = 70$, the general behavior is a direct reflection of the measured size dependence.

We think that the increase originates from the fact that the formation of four- to seven-membered complexes is simply facilitated by larger clusters. The decrease is caused by the increasing number of 4-coordinated molecules. In addition, the ratio $R(3/4)$ of 3-coordinated to 4-coordinated molecules in the amorphous surface range was found to be 0.47 for $n = 600$ and 0.50 for $n = 931$, and thus close to the value of 0.48 obtained for $n = 293$, but smaller than those for $n = 48$ (1.1) and $n = 123$ (0.78). Thus the number of 3-coordinated loosely bound groups of molecules is very probably also responsible for the levelling-off of the size dependence at $n = 300$.

VI. Summary and Conclusions

Significant past effort was devoted by us, and by others, to detect and analyze spectra and structures of the lowest energy states for size-selected water clusters. For larger clusters, in the size range of tens to thousands of molecules, the lowest energy state for each specific size is likely to be of lesser interest. This is since (a) both in experimental setups and in nature one encounters distributions of sizes and structures, (b) listing all the low-lying states, and ordering them according to energy would require computational methods and empirical potentials of currently unavailable accuracy. Thus it appears more meaningful to address the *qualitative* cluster characteristics as a function of mean size.

In the present molecular beam study, the cluster size distribution was determined by doping the clusters with single Na atoms which are detected by photoionization close to the threshold.[58] Vibrational predissociation cluster spectra were then investigated in the mean size range of tens to thousands of molecules. Vibrational excitation in the OH-stretch region results in photodesorption of cluster fragments from the parent cluster surface; the desorbing fragments are detected by a quadrupole mass filter with electron bombardment source. Among the photodesorption products, there is a strikingly large abundance of water hexamers, and (to a lesser extent) pentamers and tetramers. With cold parent clusters, the hexamers are easily detected, while dimers are undetectable; in a warm beam the respective signals are similar. This is in contrast to the fragment distribution expected for simple evaporation; there, a monomer is expected to be the main product, with rapid falloff as a function of size. Thus the photodesorption mechanism appears to correspond to some kind of complex collective event, in which OH excitation is channeled to intermolecular motion of a group of surface molecules, away from the rest of the cluster.

While the exact mechanism of this interesting process is unknown, there is good qualitative agreement between the measured vibrational predissociation spectrum (measured from intensity of fragments) and the computed infrared absorption spectrum of the outer cluster surface. That spectrum, which is dominated by 3-coordinated DDA and DAA molecules, differs considerably from the infrared spectrum of the entire cluster. Moreover, it differs substantially from the surface spectrum deduced from the analysis of FTIR spectra in a cold condensation cell;[55] this is since the method employed in that study associated a significantly thicker layer of molecules with the surface.

The efficiency of the photodesorption curves of Figure 4 is insensitive to the two excitation frequencies. On the other hand, there is high sensitivity to the parent cluster size. The intensity of the fragments rises from $\langle n \rangle = 25$ to a peak at about $\langle n \rangle = 70$, and falls off to about $\langle n \rangle = 300$ where a long tail begins. At the low end of the cluster size range, water clusters are known to be amorphous, while starting from $n \sim 300$ the clusters were shown to be characterized by a crystal core and a disordered surface.[54,56,57] Apparently the photofragment method with the preferential detection of products larger than dimers is mainly sensitive to amorphous structures. The molecules that are able to convert the absorbed IR-photon into the intermolecular motion are mainly connected 3-coordinated molecules that are located near the surface. This number increases with increasing cluster size and explains the rise in the size dependence curve. The drop is explained by the increasing fraction of 4-coordinated molecules which hinders the formation of larger complexes generated from 3-coordinated molecules. Finally, this number approaches a constant value, which also explains the leveling-off in the size dependence.

Appendix: MD simulations

To learn something about the fragmentation of large water clusters, we performed molecular dynamics calculations for $n = 100$ and $n = 1000$. The excitation mechanism preceding the fragmentation was conceived to heat the cluster locally, starting from a molecule considered as "excitation center". The rest of the molecules have been assigned internal vibrational energies decreasing exponentially with the distance from the "excitation center".

The H_2O monomer has been considered flexible and its interactions have been modeled by the TIP4P potential of Jorgensen et al.,[77] which was intensively used in the past two decades in simulations of aqueous solutions and clusters and gave reasonable results.[13] The flexibility of the H_2O monomer was ensured by adding intramolecular potential terms to account for the two OH stretching and the HOH bending coordinates:

$$V_{H_2O} = \frac{k_s}{2}(\delta r_{OH_1}^2 + \delta r_{OH_2}^2) + \frac{k_b}{2}\delta\varphi_{H_1OH_2}^2$$

where δr_{OH_i} represents the instantaneous deviation from the equilibrium OH_i bond length, while $\delta\varphi_{H_iOH_j}$ is the instantaneous deviation from the equilibrium H_1OH_2 bend angle. The values of the elastic constants are $k_s = 47.512$ eV/Å^2 and $k_b = 3.809$ eV.[80] We used the Verlet algorithm with a time step of 0.5 fs, typically ensuring a relative energy conservation error of the order 10^{-4}.

The fragmentation profiles for $(H_2O)_{100}$ have been averaged over 100 fragmentations, starting from random locations of the

Infrared Predissociation Spectroscopy
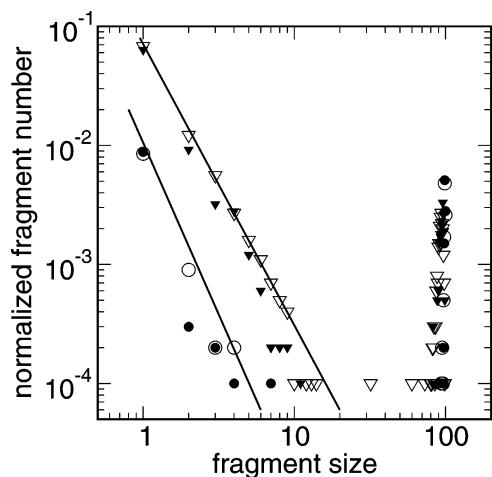
J. Phys. Chem. A, Vol. 108, No. 29, 2004 **6173**

Figure 10. Calculated distribution of fragments after excitation of the $(H_2O)_{100}$ cluster from MD simulations. Open characters: surface; filled characters: interior; circles: 1000 K; triangles: 1330 K.

initial "excitation center". In the case of $(H_2O)_{1000}$, the considered ensemble comprised only 50 fragmentations, due to the appreciable computational effort. The results for $n = 100$ are displayed in Figure 10. Here we have plotted the number of fragments $P_n(s)$ normalized such that $\sum_s sP_n(s) = 1$ as function of the fragment size s. In this way the fragment distribution is normalized to both the cluster size and the size of the ensemble.[69] The excitation was carried out for surface (open characters) and inner (full characters) positions of the molecule and final cluster temperatures of 1000 K (circles) and 1330 K (triangles). These values correspond to local excitation energies of about 60 and 80 vibrational quanta of 3400 cm^{-1} into the water molecules and thus take into account the IR excitation and the zero point energies. They are in the range of the lowest temperatures for which evaporation could be observed. The distribution consists of peaks around the initial cluster size $n = 100$ and a series of small fragments which decay over more than 2 orders of magnitude. The fragment distributions are dominated by the small fragments. The distributions for larger excitation energies imply higher intensities for smaller fragments. The results are only slightly dependent on the initial position giving surface excitations a higher probability than inner ones. This behavior continues in the same way for the larger clusters $\langle n \rangle = 1000$, not shown in Figure 10. Fragments up to the size of $s = 10$ are observed. We note that that this result which is in disagreement with the experiments on the IR excitation does not depend on the model. Similar results were obtained using rigid molecules and the SHAKE algorithm.

References and Notes

(1) Walrafen, G. E. *J. Chem. Phys.* **1967**, *47*, 114.

(2) Bertie, J. E.; Lan, Z. *Appl. Spectrosc.* **1996**, *50*, 1047.

(3) Bergren, M. S.; Schuh, D.; Sceats, M. G.; Rice, S. A. *J. Chem. Phys.* **1978**, *69*, 3477.

(4) Baragiola, R. A. In *Water in Confining Geometries*; Buch, V., Devlin, J. P., Eds.; Springer: Berlin, 2003; p 359.

(5) Buch, V.; Devlin, J. P. *J. Chem. Phys.* **1999**, *110*, 3437.

(6) Buck, U.; Huisken, F. *Chem. Rev.* **2000**, *100*, 3863.

(7) Huang, Z. S.; Miller, R. E. *J. Chem. Phys.* **1989**, *91*, 6613.

(8) Huisken, F.; Kaloudis, M.; Kulcke, A. *J. Chem. Phys.* **1996**, *104*, 17−25.

(9) Buck, U.; Ettischer, I.; Melzer, M.; Buch, V.; Sadlej, J. *Phys. Rev. Lett.* **1998**, *80*, 2578.

(10) Brudermann, J.; Melzer, M.; Buck, U.; Kazimirski, J.; Sadlej, J.; Buch, V. *J. Chem. Phys.* **1999**, *110*, 10649.

(11) Sadlej, J.; Buch, V.; Kazimirski, J.; Buck, U. *J. Phys. Chem. A* **1999**, *103*, 4933.

(12) Brudermann, J.; Buck, U.; Buch, V. *J. Phys. Chem.* **2002**, *106*, 453.

(13) Burnham, C. J.; Xantheas, S. S. *J. Chem. Phys.* **2002**, *116*, 1479.

(14) Buck, U.; Ettischer, I.; Melzer, M.; Buch, V.; Sadlej, J. *Phys. Rev. Lett.* **1998**, *80*, 2578.

(15) Kim, K.; Jordan, K. D.; Zwier, T. S. *J. Am. Chem. Soc.* **1994**, *116*, 11568.

(16) Gregory, J. K.; Clary, D. C. *J. Chem. Phys.* **1996**, *105*, 6626.

(17) Kim, J.; Kim, K. S. *J. Chem. Phys.* **1998**, *109*, 5886.

(18) Gregory, J. K.; Clary, D. C. In *Advances in Molecular Vibrations and Collision Dynamics*; Bowman, J., Bačić, Z., Eds.; JAI Press Inc.: Stamford, 1998; p 311.

(19) Liu, K.; Cruzan, J. D.; Saykally, R. J. *Science* **1996**, *271*, 929.

(20) Nauta, K.; Miller, R. E. *Science* **2000**, *287*, 293.

(21) Steinbach, C.; Andersson, P.; Melzer, M.; Buck, U.; Buch, V. *Phys. Chem. Phys.*, in press.

(22) Keutsch, F. N.; Saykally, R. J. *Proc. Natl. Acad. Sci. U.S.A.* **2001**, *98*, 10533.

(23) Cruzan, J. D.; Brown, M. G.; Liu, K.; Braly, L. B.; Saykally, R. J. *J. Chem. Phys.* **1996**, *105*, 6634.

(24) Liu, K.; Brown, M. G.; Saykally, R. J. *J. Phys. Chem.* **1997**, *101*, 8995.

(25) Viant, M. R.; Cruzan, J. D.; Lucas, D. D.; Brown, M. G.; Liu, K.; Saykally, R. J. *J. Phys. Chem. A* **1997**, *101*, 9032.

(26) Groenenboom, G. C.; Wormer, P. E. S.; van der Avoird, A.; Mas, E. M.; Bukowski, R.; Szalewicz, K. *J. Chem. Phys.* **2000**, *113*, 6702.

(27) Pribble, R. N.; Zwier, T. S. *Science* **1994**, *265*, 75.

(28) Gruenloh, C. J.; Carney, J. R.; Arrington, C. A.; Zwier, T. S.; Fredericks, S. Y.; Jordan, K. D. *Science* **1997**, *276*, 1678.

(29) Gruenloh, C. J.; Carney, J. R.; Hagemeister, F. C.; Arrington, C. A.; Fredericks, S. Y.; Zwier, T. S.; Wood, J. T., III; Jordan, K. D. *J. Chem. Phys.* **1998**, *109*, 6601.

(30) Gruenloh, C. J.; Carney, J. R.; Hagemeister, F. C.; Zwier, T. S.; Wood, J. T., III; Jordan, K. D. *J. Chem. Phys.* **2000**, *113*, 2290.

(31) Watanabe, T.; Ebata, T.; Tanabe, S.; Mikami, N. *J. Chem. Phys.* **1996**, *105*, 408.

(32) Roth, W.; Schmitt, M.; Jacoby, C.; Spangenberg, D.; Janzen, C.; Kleinermanns, K. *Chem. Phys.* **1998**, *239*, 1.

(33) Janzen, C.; Spangenberg, D.; Roth, W.; Kleinermanns, K. *J. Chem. Phys.* **1999**, *110*, 9898.

(34) Barth, H. D.; Buchhold, K.; Djafari, S.; Reimann, B.; Lommatzsch, U.; Brutschy, B. *Chem. Phys.* **1998**, *239*, 49.

(35) Farantos, S. C.; Kapetanikis, S.; Vegiri, A. *J. Phys. Chem.* **1993**, *97*, 12158.

(36) Tsai, C. J.; Jordan, K. D. *J. Phys. Chem.* **1993**, *97*, 5208.

(37) Kahn, A. *J. Phys. Chem.* **1995**, *99*, 12450.

(38) Lee, C.; Chen, H.; Fitzgerald, G. *J. Chem. Phys.* **1995**, *102*, 1266.

(39) Sremaniak, L. S.; Perera, L.; Berkowitz, M. L. *J. Chem. Phys.* **1996**, *105*, 3715.

(40) Wales, D. J.; Hodges, M. P. *Chem. Phys. Lett.* **1998**, *286*, 65.

(41) Sadlej, J. *Chem. Phys. Lett.* **2001**, *333*, 485.

(42) Hartke, B. *Phys. Chem. Chem. Phys.* **2003**, *5*, 275.

(43) Vernon, M. F.; Krajnovich, D. J.; Kwok, H. S.; Lisy, J. M.; Shen, Y. R.; Lee, Y. T. *J. Chem. Phys.* **1982**, *77*, 47.

(44) Coker, D. F.; Miller, R. E.; Watts, R. O. *J. Chem. Phys.* **1985**, *82*, 3554.

(45) Page, R.; Vernon, M. F.; Shen, Y. R.; Lee, Y. T. *Chem. Phys. Lett.* **1987**, *141*, 1.

(46) Paul, J. B.; Collier, C. P.; Saykally, R. J.; Scherrer, J. J.; O'Keefe, A. *J. Phys. Chem.* **1997**, *101*, 5211.

(47) Goss, L. M.; Sharpe, S. W.; Blake, T. A.; Vaida, V.; Brault, J. W. *J. Phys. Chem. A* **1999**, *103*, 103.

(48) Bauerecker, S. **2003**, unpublished results.

(49) Torchet, G.; Schwartz, P.; Farges, J.; de Feraudy, M. F.; Raoult, B. *J. Chem. Phys.* **1983**, *79*, 6196.

(50) Huang, J.; Bartell, L. S. *J. Chem. Phys.* **1995**, *99*, 3924.

(51) Bartell, L. S.; Chushak, Y. G. In *Water in Confining Geometries*; Buch, V., Devlin, J. P., Eds.; Springer: Berlin, 2003; p 399.

(52) Rowland, B.; Kadagathur, N. S.; Devlin, J. P.; Buch, V.; Feldmann, T.; Wojcik, M. J. *J. Chem. Phys.* **1995**, *102*, 8328.

(53) Delzeit, L.; Devlin, J. P.; Buch, V. *J. Chem. Phys.* **1997**, *107*, 3726.

(54) Devlin, J. P.; Joyce, C.; Buch, V. *J. Phys. Chem. A* **2000**, *104*, 1974.

(55) Devlin, J. P.; Sadlej, J.; Buch, V. *J. Phys. Chem. A* **2001**, *105*, 974.

(56) Kazimirski, J. K.; Buch, V. *J. Phys. Chem. A* **2003**, *107*, 9762.

(57) Devlin, J. P.; Buch, V. In *Water in Confining Geometries*; Buch, V., Devlin, J. P., Eds.; Springer: Berlin, 2003; p 425.

(58) Bobbert, C.; Schütte, S.; Steinbach, C.; Buck, U. *Eur. Phys. J. D* **2002**, *19*, 183.

(59) Huisken, F.; Mohammad-Pooran, S.; Werhahn, O. *Chem. Phys.* **1998**, *239*, 11−22.

(60) Buck, U.; Ettischer, I.; Melzer, M.; Buch, V.; Sadlej, J. *Phys. Rev. Lett.* **1998**, *80*, 2578.

(61) Buch, V.; Baurecker, S.; Devlin, J. P.; Kazimirski, J. K.; Buck, U. *Int. Rev. Phys. Chem.,* in preparation.

(62) Andersson, P.; Steinbach, C.; Buck, U. *Eur. Phys. J. D* **2003**, *24*, 53.

(63) Buck, U.; Steinbach, C. In *Water in Confining Geometries*; Buch, V., Devlin, J. P., Eds.; Springer: Berlin, 2003; p 53.

(64) Buck, U.; Gu, X. J.; Lauenstein, C.; Rudolph, A. *J. Chem. Phys.* **1990**, *92*, 6017.

(65) Buck, U.; Ettischer, I. *J. Chem. Phys.* **1998**, *108*, 33.

(66) Hagena, O. F. *Surf. Sci.* **1981**, *106*, 101.

(67) Hagena, O. F. *Z. Phys. D* **1987**, *4*, 291.

(68) Buck, U.; Winter, M. *Z. Phys. D* **1994**, *31*, 291.

(69) Beu, T. A.; Steinbach, C.; Buck, U. *Eur. Phys. J. D* **2003**, *27*, 223.

(70) Ewing, G. E. *Chem. Phys.* **1978**, *29*, 253.

(71) Beswick, J. A.; Jortner, J. *Adv. Chem. Phys.* **1981**, *47*, 363.

(72) Buck, U. In *Dynamical Processes in Molecular Physics*; Delgado-Barrio, G., Ed.; IOP: Bristol, 1993; p 275.

(73) Brudermann, J.; Lohbrandt, P.; Buck, U.; Buch, V. *J. Chem. Phys.* **2000**, *112*, 11038.

(74) Hermansson, K.; Lingren, J.; Probst, M. M. *Chem. Phys. Lett.* **1995**, *233*, 371.

(75) Buch, V.; Sandler, P.; Sadlej, J. *J. Phys. Chem.* **1998**, *102*, 8641.

(76) Buck, U. *Adv. At. Mol. Opt. Phys.* **1995**, *35*, 121.

(77) Jorgensen, W. L.; Chandrasekhar, J.; Madura, J. D.; Impey, R. W.; Klein, M. L. *J. Chem. Phys.* **1983**, *79*, 926.

(78) Nielson, G.; Townsend, R. M.; Rice, S. A. *J. Chem. Phys.* **1984**, *81*, 5288.

(79) Nienhuys, H.-K.; Woutersen, S.; van Santen, R. A.; Bakker, H. J. *J. Chem. Phys.* **1999**, *111*, 1494.

(80) Herzberg, G. *Molecular Spectra and Molecular Structure, II. Infrared and Raman Spectra of Polyatomic Molecules*; Van Nostrand Reinhold: New York, 1950.